Ab initio calculation of electronic and optical properties of metallic tin

2009 J. Phys.: Condens. Matter 21 115502

(http://iopscience.iop.org/0953-8984/21/11/115502)

J. Phys.: Condens. Matter **21** (2009) 115502 (5pp) doi:10.1088/0953-8984/21/11/115502

Ab initio calculation of electronic and optical properties of metallic tin

Thomas G Pedersen[1,2], Paritosh Modak[3,4], Kjeld Pedersen[1,2], Niels E Christensen[3], Mads M Kjeldsen[2,3] and Arne Nylandsted Larsen[2,3]

[1] Department of Physics and Nanotechnology, Aalborg University, DK-9220 Aalborg Øst, Denmark
[2] Interdisciplinary Nanoscience Center (iNANO), Denmark
[3] Department of Physics and Astronomy, University of Aarhus, DK-8000 Aarhus C, Denmark

Received 27 October 2008, in final form 2 February 2009
Published 20 February 2009
Online at stacks.iop.org/JPhysCM/21/115502

Abstract
The electronic and optical properties of the metallic bcc and β-Sn phases of tin are studied using density functional theory. The effects of spin–orbit coupling are examined and significant splittings are found in the band structures for both phases. Based on *ab initio* band structures we calculate the anisotropic optical response of β-Sn. Both intra- and interband contributions are included and the plasma frequencies for both the ordinary and extraordinary optical axis are calculated. The theoretical results are found to be in excellent agreement with experimental spectra for the anisotropic optical response. We identify the electronic transitions responsible for the dominant interband resonances in the near-infrared response.

(Some figures in this article are in colour only in the electronic version)

1. Introduction

Elementary Sn assumes several different crystal structures depending on pressure and temperature. At atmospheric pressure and temperatures below 286 K, the diamond structure (α-Sn or grey tin) is preferred. Upon raising temperature or pressure, a transition to the β-Sn or white tin structure is observed. The crystal structure of this phase is body centred tetragonal with a two-atom basis. At a pressure of approximately 95 kbar [1], a body centred tetragonal phase appears and eventually (above approximately 400 kbar) Sn assumes a body centred cubic (bcc) structure [2]. Among these structures, α-Sn is a zero band gap semiconductor whereas the remaining phases are metallic.

The structural properties of Sn have been studied theoretically using density functional theory (DFT) and muffin-tin methods in several publications [3–8]. Information on the band structure of the metallic phases is limited, however. The only available *ab initio* energy band structures of the β-Sn [3] and bcc Sn [6] do not include spin–orbit interaction (SOI), which is expected to be important. In addition, empirical pseudopotential band structures for β-Sn exist [9, 10]. In the present work, the electronic structure of the metallic β-Sn and bcc Sn phases is investigated using DFT. The effect of SOI is studied for both phases. Based on the *ab initio* band structures, the plasma frequency and interband dielectric constant are computed. As the β-Sn structure is uniaxially anisotropic, optical constants for polarization parallel and perpendicular to the crystal c-axis are calculated. The theoretical spectra are compared to experimental values [11] of the imaginary part of the dielectric constant for β-Sn for both polarizations. The influence of SOI on the intraband response is found to be noticeable with changes of the plasma frequency around 0.2 eV. Our theoretical interband response is in excellent agreement with experiments. The determination of the anisotropic dielectric constant allows us to predict plasmon resonances in various geometries. As an example, the present results are applied to nanoparticles in water and again excellent agreement with experiments is demonstrated.

[4] Permanent address: Purnima Laboratories, High Pressure Physics Division, Bhabha Atomic Research Centre, Trombay, Mumbai-400085, India.

2. Electronic structure

Our electronic structure calculations were done using the *Abinit* plane wave [12] and WIEN2k [13] DFT codes. All *Abinit* results were obtained using 12 × 12 × 12 Monkhorst–Pack grids and 25 hartree plane wave cut-off energy. We

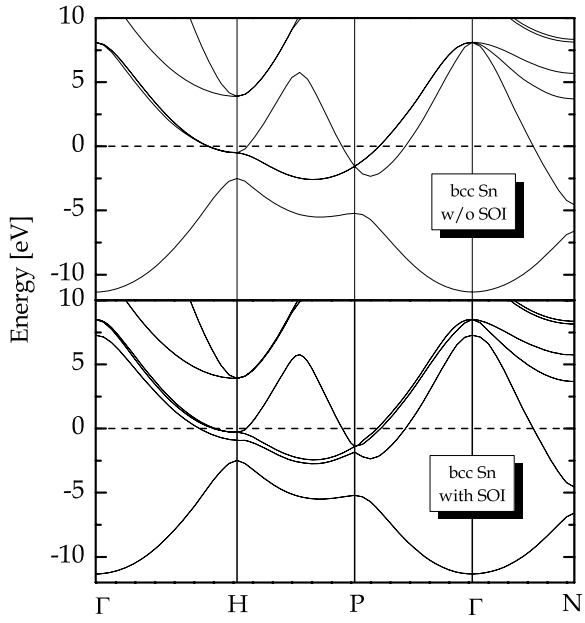

Figure 1. Energy band structure of bcc Sn in the equilibrium geometry with (lower panel) and without (upper panel) spin–orbit interaction. Fermi level at 0 eV.

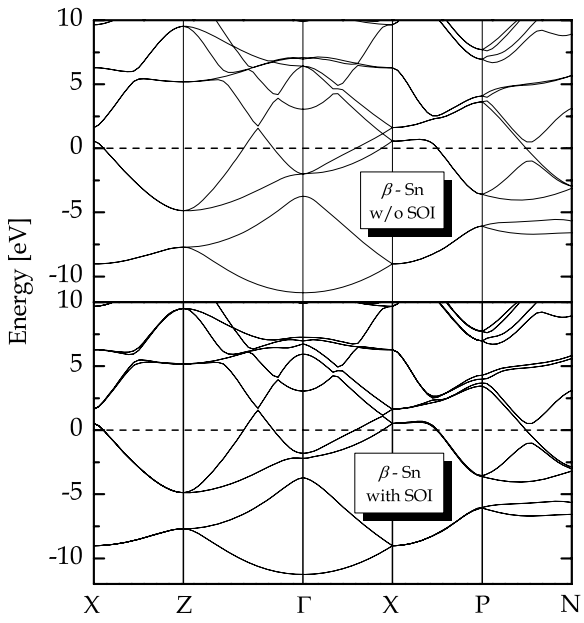

Figure 2. Energy band structure of β-Sn in the experimental geometry with (lower panel) and without (upper panel) spin–orbit interaction. Fermi level at 0 eV.

used the Teter–Pade parametrization [14] and Hartwigsen–Goedecker–Hutter (HGH) pseudopotentials [15] treating the 4d states as core states. Plasma frequencies were computed using tetrahedron integration with 2601 k-points in the irreducible wedge of the Brillouin zone (BZ) based on the *Abinit* DFT band structure. Calculations were performed with and without including SOI in order to quantify its importance. The *Abinit* code does not allow for computation of interband optical response of metals, however. Hence, for the calculation of the interband response the WIEN2k code was applied instead. For self-consistent electronic structure calculations using the WIEN2k code we have used $R_{\mathrm{mt}}K_{\max} = 9$ and a total of 5000 k-points for the BZ integration. For exchange–correlation terms the Perdew–Burke–Ernzerhof (PBE) generalized gradient approximation [16] was applied and the 4d states were treated as valence states. To calculate the optical response an even denser k-mesh consisting of 20 000 k-points for the whole BZ was used. We have checked that all applied k-meshes are sufficient for convergence. All calculations were done using the experimental lattice constants for β-Sn ($a = 10.98$ Bohr and $c = 5.97$ Bohr [17]) and the equilibrium value ($a = 7.09$ Bohr [5]) for bcc Sn at zero pressure. While β-Sn is the stable phase at zero pressure, the bcc results are included in order to estimate the sensitivity of SOI splitting and plasma frequency to crystal structure.

The HGH electronic band structure is shown in figure 1 for bcc Sn and figure 2 for β-Sn. In both cases, the effect of SOI is significant, as expected for a relatively heavy element. In the bcc structure, the H_{15} level is split by 0.63 eV. In the β-Sn structure, the most pronounced effect of SOI is the Γ_6^+–Γ_7^+ splitting of 0.41 eV, roughly two-thirds the splitting in the bcc case. Our results are in qualitative agreement with earlier semi-empirical calculations [9, 10]. The SOI has only a minor influence on the density of states (DOS), especially for the occupied states, as illustrated in figure 3. Also, band structures obtained using different exchange–correlation forms were found to be practically identical.

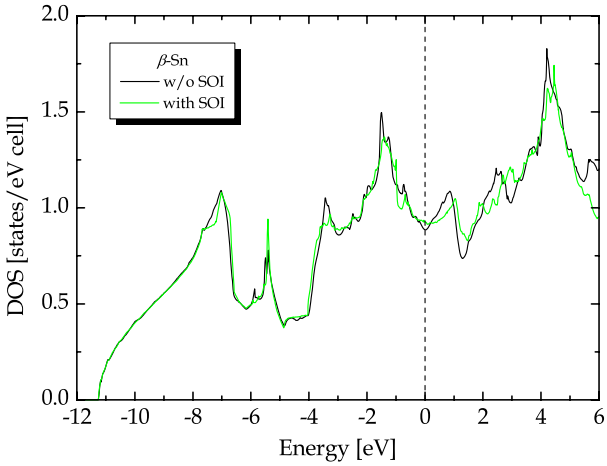

Figure 3. Density of states for β-Sn with and without SOI. The vertical dashed line indicates the Fermi level.

3. Optical properties

In general, the optical response of a metal can be decomposed into intraband and interband contributions. In addition, for an anisotropic material such as β-Sn both contributions depend on the direction of the optical polarization vector. The β-Sn structure is uniaxially anisotropic with the c-axis defining the extraordinary optical axis. Thus, all optical constants are labelled $\parallel$ or $\perp$ corresponding to the directions parallel and

Table 1. Calculated plasma frequencies for different crystal structures.

Material	SOI	Plasma frequency (eV)
bcc Sn	No	11.44
bcc Sn	Yes	11.28
β-Sn	No	9.39 ($\perp$ c-axis)
β-Sn	Yes	9.20 ($\perp$ c-axis)
β-Sn	No	8.42 ($\parallel$ c-axis)
β-Sn	Yes	8.25 ($\parallel$ c-axis)

perpendicular to the c-axis, respectively. The total dielectric constant is then $\varepsilon^\sigma(\omega) = \varepsilon^\sigma_{\text{intra}}(\omega) + \varepsilon^\sigma_{\text{inter}}(\omega)$ with $\sigma = \parallel$ or $\perp$. A general expression for the dielectric constant valid beyond the parabolic approximation for the energy dispersion is [18]

$$\varepsilon^\sigma(\omega) = 1 + \frac{e^2\hbar^2}{\varepsilon_0 m_0^2 \Omega} \sum_{i,f} \frac{[f(E_i) - f(E_f)]|\langle f|\hat{p}_\sigma|i\rangle|^2}{E_{fi}[E_{fi}^2 - \hbar^2\omega^2]}, \quad (1)$$

where Ω is the crystal volume, m_0 is the free-electron mass, f is the Fermi function, and $\hat{p}_\sigma$ is the momentum operator. Moreover, $|i\rangle$ and $|f\rangle$ are initial and final electron states, respectively, and $E_{fi} = E_f - E_i$ is their energy separation. The energy of the initial state is $E_{n\vec{k}}$, where n is the band index and $\vec{k}$ is the electron wavevector. If the wavevector of the perturbing electric field is $\vec{q}$, the final state will have an energy $E_{m,\vec{k}+\vec{q}}$. In the long wavelength approximation, $E_{m,\vec{k}+\vec{q}} \approx E_{m\vec{k}} + \nabla E_{m\vec{k}} \cdot \vec{q}$ and $f(E_{m,\vec{k}+\vec{q}}) \approx f(E_{m\vec{k}}) + f'(E_{m\vec{k}})\nabla E_{m\vec{k}} \cdot \vec{q}$, with f' the energy derivative of f. We can now convert the summation over k-points into an integral and separate interband ($m \neq n$) from intraband ($m = n$) terms. In the former, $\vec{q}$ can be disregarded and we find

$$\varepsilon^\sigma_{\text{inter}}(\omega) = \frac{e^2\hbar^2}{8\pi^3\varepsilon_0 m_0^2} \times \sum_{m>n} \int \frac{[f(E_{n\vec{k}}) - f(E_{m\vec{k}})]|\langle m\vec{k}|\hat{p}_\sigma|n\vec{k}\rangle|^2}{E_{m\vec{k},n\vec{k}}[E^2_{m\vec{k},n\vec{k}} - \hbar^2\omega^2]}\, d^3k. \quad (2)$$

In the intraband case, we notice that $\lim_{\vec{q}\to 0}[f(E_{n\vec{k}}) - f(E_{n,\vec{k}+\vec{q}})]/E_{n,\vec{k}+\vec{q},n\vec{k}} = -f'(E_{n\vec{k}})$ and utilize the relation $\langle n\vec{k}|\hat{p}_\sigma|n\vec{k}\rangle = \frac{m_0}{\hbar}\partial E_{n\vec{k}}/\partial k_\sigma$. Also, at low temperature $f'(E_{n\vec{k}}) \approx -\delta(E_{n\vec{k}} - E_F)$, where E_F is the Fermi energy. Upon taking the $\vec{q} \to 0$ limit, the intraband contribution then reduces to the Drude expression [19]

$$\varepsilon^\sigma_{\text{intra}}(\omega) = 1 - \frac{\omega^2_{p,\sigma}}{\omega(\omega + i\gamma)}, \quad (3)$$

where we have added a phenomenological broadening γ assumed independent of direction and the plasma frequency $\omega_{p,\sigma}$ is given by

$$\omega^2_{p,\sigma} = \frac{e^2}{8\pi^3\hbar^2\varepsilon_0} \sum_n \int \left(\frac{\partial E_{n\vec{k}}}{\partial k_\sigma}\right)^2 \delta(E_{n\vec{k}} - E_F)\, d^3k. \quad (4)$$

This expression can readily be evaluated using tetrahedron integration and the computed band structure. Data exported from *Abinit* have been used in a Fortran program constructed to this end and the results calculated for bcc and β-Sn are given in table 1.

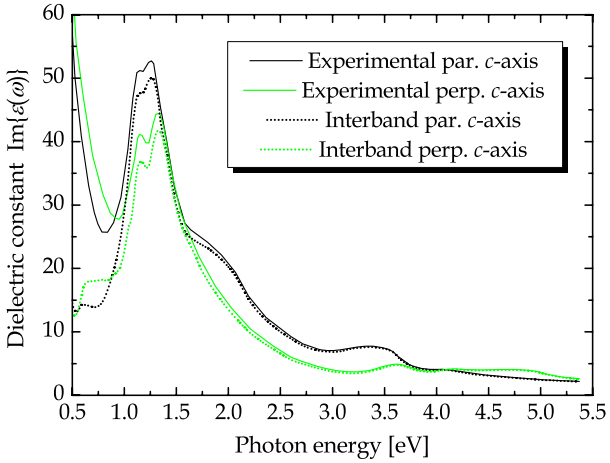

Figure 4. Experimental absorption spectra from [11] (solid curves). The dotted curves are the interband parts obtained by subtracting calculated intraband parts.

It is clear that both anisotropy and, to a lesser degree, SOI influence the plasma frequency. For free-electron like metals, the plasma frequency is $\omega_p = (e^2 n/\varepsilon_0 m)^{1/2}$ and therefore expected to depend mainly on the electron density. Hence, the difference between bcc and β-Sn results might appear surprisingly large given the nearly equal atomic volumes of the two structures. Inspection of the bcc band structure shows that for this structure the Fermi level is located near the parabolic portion of the bands. However, in the β-Sn case, the additional four valence electrons per unit cell raise the Fermi level into a highly non-parabolic portion of the band structure. This causes the reduction of the plasma frequency. It is clear that crystal structure substantially affects plasma frequencies (and SOI splittings) even though average electron densities of the two phases are nearly identical.

Knowledge of the plasma frequency makes it possible to extract an approximate interband dielectric constant from available experimental data for the total (intra + interband) response. To this end, we have used experimental data for the imaginary part of $\varepsilon^\sigma(\omega)$ from Schwarz [11]. Interband spectra are obtained by subtracting the intraband response equation (1) using the plasma frequencies of table 1 (including SOI) and taking $\hbar\gamma = 0.08$ eV. This value was selected by fitting the Drude formula equation (3) to the low-frequency tail of the experimental data, which is dominated by the intraband response due to the ω^{-1} behaviour. After subtracting the Drude term, the interband spectra in figure 4 show pronounced resonances between 1.0 and 1.4 eV. For the parallel response, additional resonances are found around 2.0 and 3.4 eV. For the perpendicular case, only a high energy resonance around 3.6 eV is observed. Finally, shoulders around 0.7 eV are found for both polarizations.

To complete the analysis of the optical response, the real part of the interband dielectric constant is needed. We obtain these spectra in two independent ways: (1) by Kramers–Kronig transformation of the experimental imaginary part of

the interband response and (2) by means of full-potential linear augmented plane wave calculations using the WIEN2k code [13]. In the latter case, the imaginary part of the response equation (2) is first computed in the limit of vanishing broadening (delta-function resonances). Subsequently, convolution with a Lorentzian line shape function (taking again $\hbar\gamma$ as the broadening) and the Kramers–Kronig transformation provides the complex dielectric constant. The first method is useful because the imaginary part is known over a wide frequency range. Note that we only transform the interband contribution in order to avoid the low-frequency singularity of the spectrum. However, the missing high-frequency part ($\hbar\omega > 5.37$ eV) must be estimated and for this purpose we fit an ω^{-3} tail to the experimental spectrum. The missing part of the spectrum below 0.5 eV is ignored.

In figure 5, we compare experimental ('semi-experimental') spectra with *ab initio* theoretical results for the interband response. Overall, a very satisfactory agreement is observed. In particular, the location of interband resonances is reproduced by theory with high accuracy. Moreover, the differences and crossings between spectra for the two polarization directions are in good agreement. The most pronounced discrepancy between theory and experimental data lies in the magnitude of the spectra. Hence, the resonance at 1.1–1.3 eV is overestimated by about 40% leading to a peak of ∼70 in contrast to the experimental values ∼50 (∥) and ∼40 (⊥). This discrepancy is also apparent in the real parts of the spectra for which the minima around 2 eV are twice as deep in the calculated curves. It might seem surprising that simple density functional methods provide such excellent agreement with experiments. However, the main effect of correlation corrections is a downward shift of the 4d states, which play a role in cohesive properties [5]. The visible and near-UV optical response ($\hbar\omega < 5$–6 eV) is not sensitive to these low lying states and, hence, insensitive to possible correlation effects. The error due to an overestimated hybridization of 4d states with other valence states is expected to be small. In general, quasiparticle corrections are expected to be less important in metals than in semiconductors. The good agreement with experiments confirms this trend in the present case, indicating that bare DFT bands are reasonable approximations to the full quasiparticle band structure in β-Sn. Moreover, quasiparticle approaches, such as the GW method, are extremely computationally demanding if dense k-point grids and SOI are required. We will attempt to address these issues in future work, however.

The most prominent features of both calculated and experimental interband spectra are the resonances at 1.1 and 1.3 eV. Our analysis allows us to provide a detailed assignment of the origin of these peaks. From the band structure shown in figure 2 it might be expected that the nearly parallel third and fourth band crossing the Fermi level along the $\Gamma \rightarrow X$ $[(0,0,0) \rightarrow (\frac{1}{2},\frac{1}{2},0)]$ line of the Brillouin zone are responsible for these features. In fact, by analysing the k-points contributing to the response between 1.0 and 1.4 eV we find that most points are significantly displaced from the $k_z = 0$ plane, as shown in figure 6. In this plot, we have collected k-points, for which allowed transitions with energies in the right range (resonance ±0.1 eV) are found. By considering separately the parallel and perpendicular response, we identify the Brillouin zone region responsible for the different interband resonances. Hence, in the plot, we distinguish between k-points contributing to the parallel (left panel) or perpendicular (right panel) response as well as contributions to the 1.1 eV (black) or 1.3 eV (green) resonance. For the parallel response the dominant transitions are all between the fourth and fifth bands. Similarly, for the perpendicular response, transitions between the fourth and fifth bands dominate the low energy peak while only the high energy (1.3 eV) resonance is attributed to transitions between the third and fourth bands. Moreover, the k-points are distributed over a significant portion of the Brillouin zone and, hence, cannot be ascribed to particular high symmetry lines or points. From figure 6 it is evident, however, that most points lie close to the $\Gamma \rightarrow X$ line when projected onto the $k_z = 0$ plane. It follows that the split resonance at 1.1–1.3 eV should not be attributed to the SOI induced splitting of energy bands near symmetry points observed in figure 2. In fact, we find that SOI splitting does not produce any clearly discernable features in the optical response. This is because the signatures of SOI split symmetry points is masked by a large 'uncritical' background originating from an extended part of the Brillouin zone. It is conceivable that modulation spectroscopy could resolve such features, however [20].

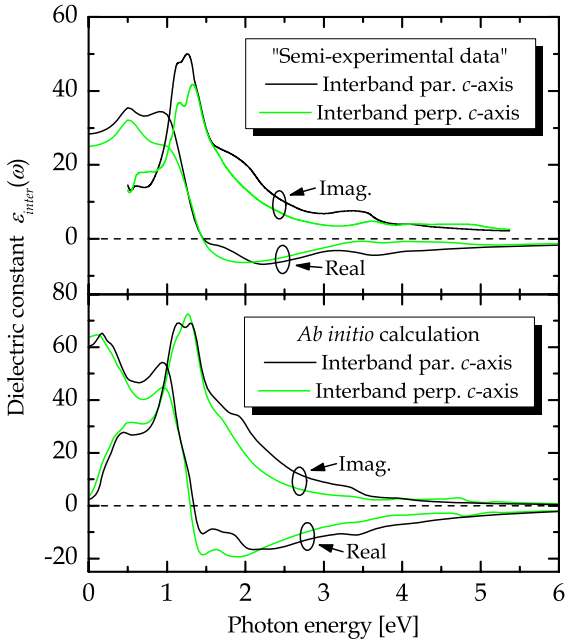

Figure 5. Comparison of semi-experimental and *ab initio* theoretical spectra for the interband response. The real parts of the semi-experimental spectra are Kramers–Kronig transforms of the imaginary parts.

The detailed analysis above provides an important link between the optical response and the electronic band structure, taking into account the influence of the uniaxial crystal structure on both intra- and interband response. However, the present results are also useful for the prediction of novel properties such as plasmon resonances in various

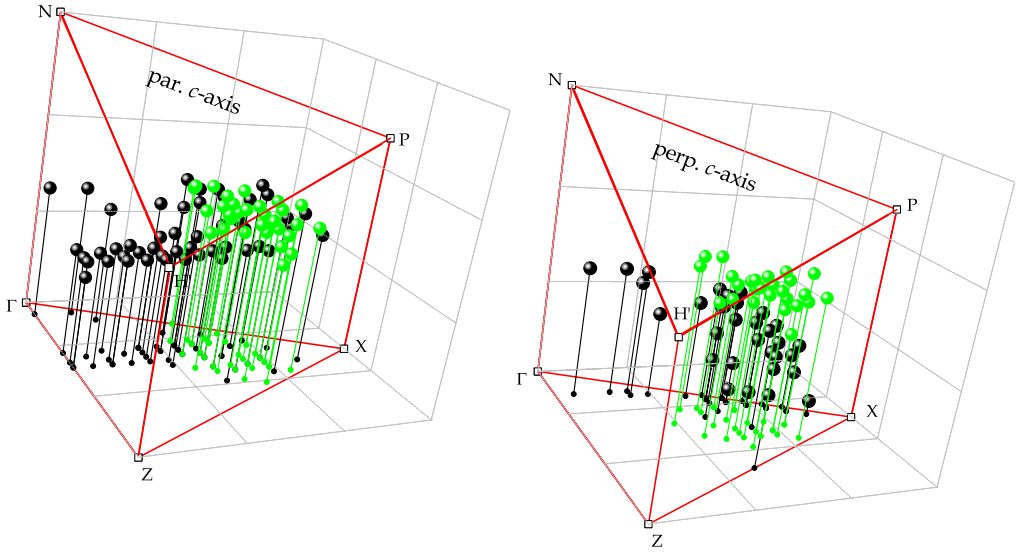

Figure 6. Distribution of k-points contributing to the interband resonances at 1.1 eV (black points) and 1.3 eV (green points) for the response parallel (left panel) and perpendicular (right panel) to the z-axis. For each point, the projection onto the $k_z = 0$ plane (small balls) is shown to help visualize the three-dimensional distribution.

geometries. As a simple example, we consider β-Sn nanospheres embedded in a host material with dielectric constant $\varepsilon_{\text{host}}$. In the Rayleigh limit appropriate for very small particles, the plasmon resonance is located at the minimum of the function $|\varepsilon^{\sigma}(\omega) + 2\varepsilon_{\text{host}}|$. Using the 'semi-experimental' data above and taking $\varepsilon_{\text{host}} = 1.5^2$ corresponding to a glass host, we find resonances at 6.0 and 6.25 eV (207 and 198 nm wavelengths) for parallel and perpendicular polarization, respectively. Similarly, for nanoparticles in water with $\varepsilon_{\text{host}} = 1.4^2$ we find 6.35 and 6.6 eV for the two polarizations. Again, this is in good agreement with available experiments [21].

4. Summary

In summary, *ab initio* computations have been performed for the electronic structure of metallic tin in the bcc and β-Sn phases. The influence of the spin–orbit interaction on the band structure has been investigated and significant band splitting along certain high symmetry lines is predicted for both structures. The electronic structure data are subsequently applied to study the optical response of the β-Sn structure for which experimental data are available. Both intra- and interband dielectric constants are evaluated and due to the uniaxial crystal structure results are given for polarization parallel and perpendicular to the c-axis. For the intraband response we find that the plasma frequencies differ substantially for the two directions and, in addition, that spin–orbit interaction leads to a small but noticeable reduction. The interband response is characterized by several resonances but dominated by a double peak in the near-infrared 1.0–1.4 eV region. Again, pronounced differences between the two polarization directions are observed. Comparison with experiments shows excellent agreement for position as well as polarization dependence of the interband resonances. Finally, plasmon resonances of β-Sn nanoparticles are estimated and again excellent agreement with measurements is demonstrated.

Acknowledgment

TGP, KP and ANL gratefully acknowledge financial support from FTP grant #274-07-0523 project SERBINA.

References

[1] Barnett J D, Bean V E and Hall H T 1966 *J. Appl. Phys.* **37** 875
[2] Olijnyk H and Holzapfel W B 1984 *J. Physique Coll.* **45** C8-153
[3] Svane A and Antoncik E 1986 *Solid State Commun.* **58** 541
[4] Cheong B H and Chang K J 1991 *Phys. Rev.* B **44** 4103
[5] Christensen N E and Methfessel M 1993 *Phys. Rev.* B **48** 5797
[6] Christensen N E 1993 *Solid State Commun.* **85** 151
[7] Aguado A 2003 *Phys. Rev.* B **67** 212104
[8] Cui S, Cai L, Feng W, Hu H, Wang C and Wang Y 2008 *Phys. Status Solidi* b **245** 53
[9] Weisz G 1966 *Phys. Rev.* **149** 504
[10] Craven J E 1969 *Phys. Rev.* **182** 693
[11] Schwarz H 1971 *Phys. Status Solidi* b **44** 603
[12] Gonze X, Beuken J-M, Caracas R, Detraux F, Fuchs M, Rignanese G-M, Sindic L, Verstraete M, Zerah G, Jollet F, Torrent M, Roy A, Mikami M, Ghosez Ph, Raty J-Y and Allan D C 2002 *Comput. Mater. Sci.* **25** 478
[13] Blaha P, Schwarz K, Madsen G K H, Kvasnicka D and Luitz J 2001 *WIEN2k, An Augmented Plane Wave Plus Local Orbitals Program for Calculating Crystal Properties* Vienna University of Technology, Austria
[14] Goedecker S, Teter M and Hutter J 1996 *Phys. Rev.* B **54** 1703
[15] Hartwigsen C, Goedecker S and Hutter J 1998 *Phys. Rev.* B **58** 3541
[16] Perdew J P, Burke K and Ernzerhof M 1996 *Phys. Rev. Lett.* **77** 3865
[17] Rayne J A and Chandrasekhar B S 1960 *Phys. Rev.* **120** 1658
[18] See e.g. Yu P Y and Cardona M 2005 *Fundamentals of Semiconductors* (Berlin: Springer)
[19] Maksimov E G, Mazin I I, Rashkeev S N and Uspenski Y A 1988 *J. Phys. F: Met. Phys.* **18** 833
[20] Christensen N E and Seraphin B O 1971 *Phys. Rev.* B **4** 3321
[21] Henglein A and Giersig M 1994 *J. Phys. Chem.* **98** 6931